A Composite Life Cycle of Nonsquall Mesoscale Convective Systems over the Tropical Ocean. Part II: Heat and Moisture Budgets

STEVEN K. ESBENSEN AND JOUGH-TAI WANG*

Department of Atmospheric Sciences, Oregon State University, Corvallis, Oregon

EDWARD I. TOLLERUD

Weather Research Program, ERL/NOAA, Boulder, Colorado

(Manuscript received 20 April 1987, in final form 19 August 1987)

ABSTRACT

The heat and moisture budgets associated with five large nonsquall cloud clusters observed during Phase 3 of the Global Atmospheric Research Program's Atlantic Tropical Experiment (GATE) are investigated. The input data for the budget computations are objectively analyzed fields of wind, temperature and relative humidity that were based on conventional upper-air soundings. Estimates of the radiative heating rate were obtained from Cox and Griffith. A compositing technique is used to summarize the budget results for the growing, mature and dissipating stages of the clusters.

The budgets in the growing stage are characterized by a very large low-level, apparent moisture sink separated in height from the region where the apparent heating is realized. In the mature stage, the apparent heating maximum shifts upward, accompanied by the development of a corresponding secondary maximum of apparent drying. A composite of radiative heating estimates from Cox and Griffith shows that the horizontal radiative heating gradients reach their maximum strength during the mature stage. In the dissipating stage, the apparent heat source is approximately balanced by the apparent moisture sink above the freezing level; below the freezing level, the implied vertical convective flux of sensible and latent heat is approximately constant with height.

The time-dependent behavior of the budgets gives support to the hypothesis of Leary and Houze that the widespread upper-level cloud decks associated with cloud clusters play an active and important role in determining large-scale heat and moisture budgets in the tropics.

1. Introduction

Observational studies have established several important characteristics of large-scale heat and moisture budgets in the presence of deep tropical convection. First, the level in the troposphere at which the large-scale flow appears to lose moisture to the condensation process is significantly below the level at which heating is realized (Yanai et al., 1973). This is a well-known consequence of the vertical transport of heat by cumulus clouds in relatively undilute cumulonimbus cores (Riehl and Malkus, 1958). Second, the radiative heating term is the same order of magnitude as the vertical convergence of the vertical eddy heat flux by deep convection (e.g., Yanai et al., 1973), indicating that radiation can play an important role in determining the amount of convective activity over a large-scale region in the tropics.

More recently, attention has been focused on the role of the mesoscale anvil clouds that accompany active convective cells in cloud clusters. Large-scale budget studies alone cannot unambiguously separate the effects of the convection and the anvil clouds. But since there is a time lag between the initial development of the convective cells and the associated anvil cloud, heat and moisture budgets with a time resolution on the order of hours can be used to infer some of the properties of the anvil clouds. This approach has been used by Frank (1979) in examining the vertically integrated budgets during all three phases of GATE.

The value of computing large-scale heat and moisture budgets from a network of upper-air soundings comes from the ability to integrate over time and space domains that are not available from other data sources. For example, satellite data can provide a great deal of information on the horizontal structure of mesoscale systems, but only at selected levels. Meteorological radars can provide detailed information on such basic parameters as the wind and precipitation fields, but only in a limited part of a convective system. In situ sensors aboard aircraft can measure all of the atmospheric variables that are relevant for large-scale budget computations, but only along the flight tracks. In the

* Present affiliation: Climate Systems Research Program, College of Geosciences, Texas A&M University, College Station, TX 77843.

Corresponding author address: Dr. Steven K. Esbensen, Dept. of Atmospheric Sciences, Oregon State University, Corvallis, OR 97331.

future, data assimilation techniques may provide a satisfactory method for combining all of these data sources into a single set of analyzed fields. At present, however, large-scale budgets provide independent information and a context for interpreting the more detailed measurements.

The purpose of this paper is to add to the observational knowledge of nonsquall cloud clusters by presenting composited heat and moisture budgets that summarize the life cycles of five large cloud clusters during Phase 3 of GATE. Based on previous studies, we anticipate that the cloud clusters will have significant effects on the heat and moisture budgets. In Tollerud and Esbensen (1985; hereafter referred to as Part I), we found that the evolution of the vertical motion field in the growing, mature and dissipating stages of the clusters was similar to the life cycle hypothesized by Leary and Houze (1979) for the individual mesoscale precipitation features that combined to form the nonsquall clusters. Strong upward motion developed in the upper troposphere from the growing to the mature stage; in the lower troposphere, the upward velocities decreased dramatically from the mature to the dissipating stage. This is consistent with time-dependent mass budgets of Frank (1978) and the results of Johnson and Young (1983) for anvil clouds in winter monsoon clusters near Borneo.

In sections 2 and 3 we discuss the data sources and the methodology employed in this study. The density of the upper-air data, and our method of analysis, make it possible for us to quantitatively examine features of the nonsquall cloud clusters which are intermediate in scale between the synoptic-scale flow and the mesoscale precipitation features: the so-called meso-α scale. Our calculations follow these intermediate-scale features by using the full upper-air dataset from the convective subprogram of GATE, including the winds from the B-array ships. The radiation term of the heat budget is evaluated by using the three-dimensional radiative heating estimates from Cox and Griffith (1979). Section 4 presents the composite heat and moisture budgets of the five nonsquall convective systems. Concluding remarks are found in section 5.

2. Datasets

a. Upper-air data

The upper-air data used in this study were obtained by optimum interpolation of the wind, temperature and relative humidity observations made over the A/B and B ship arrays during Phase 3 of GATE (see Fig. 1, Part I). The guiding principles and theoretical basis of the analysis scheme used for the analysis are described by Ooyama (1987). The goal of the analysis was to determine the horizontal wind, temperature and humidity fields that would include all of the information on the space and time scales of the available soundings, without the undesirable effects of temporal and spatial aliasing. Ooyama applied the method to the wind soundings while one of the present authors (SKE) analyzed the thermodynamic data.

The wind dataset used in this study is identical to the set used in Part I. The thermodynamic dataset contains values of the temperature and relative humidity fields archived on the same grid as the wind data. The grid consists of a ½° × ½° latitude–longitude mesh in the horizontal and 41 constant pressure levels in the vertical, from 1012 mb to 70 mb. Both datasets are archived at NCAR and are available to interested researchers.

The primary datasets chosen for the analysis of temperature and relative humidity were the B and C-scale soundings contained in the final upper-air set prepared in the United States by the Convective Subprogram Data Center (CSDC), and the upper-air dataset prepared by the National Processing Center (NPC) of the All-Union Scientific Research Institute of Hydrometeorological Information, U.S.S.R. Some subjective procedures were required in preparing these soundings for analysis using Ooyama's (1987) method. In addition to a careful manual editing of individual soundings, the phase-mean temperature and relative humidity data for each ship were adjusted to remove the most obvious biases identified through intercomparisons of data among the ships in the GATE central ship arrays. The suggestions of Reeves and Esbensen (1977) were followed to remove the effects of the pressure–height bias of the soundings in the A/B array. In the adjustment process, the phase-mean soundings from the *Quadra*, *Researcher* and *Oceanographer* served as references for the vertical structure, while the horizontal gradients were essentially determined by the A/B array soundings after removal of the pressure–height bias. For the mechanical analysis of the time-varying part of the norm field (containing disturbances with periods longer than 8 d), the derivatives of the temperature field were constrained to be consistent with the thermal wind relation in areas of low data density near the horizontal boundaries of the analysis domain. Otherwise the analysis proceeded as outlined by Ooyama (1987).

No explicit correction was made to the data as it came from the national processing centers to remove the spurious part of the diurnal variation caused by solar heating of the thermistor or the hygristor. The objective analysis method resulted in a more homogeneous phase and amplitude of the diurnal cycle over the array, particularly at lower levels. At upper levels, however, the analyzed amplitude of the diurnal temperature cycle is ~0.2°–0.4°C. The diurnal variation of the analyzed field near the ships in the B array is approximately ½ of the variation near the ships in the A/B array. This apparently unrealistic difference must be kept in mind when interpreting the composited results since there is a clear diurnal variation in the time of occurrence of the nonsquall cloud clusters (see Part I, Fig. 2).

b. Cloud cover and radiative heating estimates

The dataset produced by Cox and Griffith (1979) has been used in two ways in this study. As in Part I, the gridded cloud-cover data are used to identify the location and the life-cycle stages of the cloud clusters. In addition, the net radiative flux convergence estimates are used to produce three-dimensional estimates of the radiative heating term, Q_R, on the same grid as the wind, temperature and relative humidity data. In the horizontal direction, Cox and Griffith (1979) provide hourly flux convergence estimates on the same ½° × ½° latitude–longitude mesh as our analyzed upper-air data. In the vertical direction, averaged Q_R estimates are provided for 100 mb layers from 100 to 1000 mb and for the layer between 1000 mb and the surface. To interpolate these values to our analysis grid, the flux convergence estimates by Cox and Griffith were used to obtain a continuous radiative flux profile at each ½° × ½° horizontal grid location. Layer-averaged flux convergence values centered on the constant-pressure levels of our analysis grid were then calculated from the continuous profiles.

c. Surface marine meteorological data

Estimates of surface sensible and latent heat fluxes were calculated for each of the ships used in our upper-air data analysis using the hourly WMO surface marine meteorological data contained in the GATE data archive at the World Data Center A (Asheville, NC). This data was subjected to additional quality checks and editing by J. Meitín and K. V. Ooyama at the National Center for Atmospheric Research, Boulder, CO.

3. Methodology

a. Compositing

The compositing strategy that was used in Part I and in the present study was developed by Tollerud and Esbensen (1983). Cloud cover in the 100 to 300 mb layer as determined by Cox and Griffith (1979) was used to isolate the anvil clouds of the largest and most active systems. Only features for which the cloud cover was at least 90% over a simply connected horizontal area of 200 × 200 km^2, and persisted for at least 6 h, were considered. Five nonsquall systems met the size and duration criteria during the period from 31 August through 17 September 1974 (see Table 1).

The life cycle of each system was broken into three stages: growing, mature and dissipating. In the growing stage, the anvil first appears and grows rapidly. During the mature stage, the anvil attains its greatest horizontal extent and remains approximately the same size. In the dissipating stage the anvil begins to break up and eventually disappears.

The terms in the heat and moisture budgets were first computed on the full grid at the 3-hourly analysis times for the upper-air data. The Q_R estimates were obtained by an arithmetic average over the 3 hours centered on the upper-air analysis time. The budget terms were then composited on a ½° × ½° latitude–longitude grid centered on the cluster for the growing, mature and dissipating stages. See Part I and Tollerud and Esbensen (1983) for further details.

TABLE 1. Nonsquall clusters included in composite.

Cluster number	Time/Date*	Center location, mature stage (°N, °W)
1	1200/02–0300/03	8, 25
2	0000/05–2100/05	9.5, 21
3	0600/05–0000/06	9, 25.5
4	1200/16–0300/17	9, 21
5	2100/16–1200/17	10, 25

* Times are in UTC and dates are for September 1974.

b. Budget equations

The heat and water vapor budgets are cast in the commonly used form

$$Q_1 = \frac{\partial}{\partial t}(c_pT) + \mathbf{V}\cdot\nabla(c_pT) + \omega\frac{\partial}{\partial p}(c_pT + \phi) \quad (1)$$

$$Q_2 = -L_v\left(\frac{\partial q}{\partial t} + \mathbf{V}\cdot\nabla q + \omega\frac{\partial q}{\partial p}\right), \quad (2)$$

where Q_1 and Q_2 are respectively the apparent heat source and the apparent moisture sink expressed in energy units. Here, p, $\mathbf{V}$, ω, T, ϕ and q are the air pressure, the horizontal wind velocity, the vertical "p" velocity, temperature, geopotential and the specific humidity. The specific heat at constant pressure, c_p, and the latent heat of vaporization, L_v, are held constant; Q_1 and Q_2 are explicitly calculated from the objectively analyzed upper-air data.

Using Q_1 and Q_2, the first law of thermodynamics and the moisture continuity equation may be written in the approximate forms

$$Q_1 = Q_R + \frac{\partial}{\partial p}(gF_s) + L_v(c - e) + L_s(d - s) + L_f(f - m) \quad (3)$$

$$-Q_2/L_v = \frac{\partial}{\partial p}(gF_q) - (c - e) - (d - s), \quad (4)$$

where Q_R, F_s and F_q are the radiative heating rate and the upward vertical flux of sensible heat and water vapor per unit mass, respectively. The variables c, e, f, m, d and s are the condensation, evaporation, freezing, melting, deposition and sublimation rates, respectively; L_f ($=L_s - L_v$) is the latent heat of fusion. Equations

(3)–(4) differ from early budget studies (e.g., Yanai et al., 1973) by the inclusion of phase transitions involving ice; similar equations have been used diagnostically by Houze (1982) and Johnson and Young (1983). Summing (3) and $L_v \times$ (4), we obtain

$$Q_1 - Q_2 - Q_R = \frac{\partial}{\partial p}(gF_h) + L_f(f - m + d - s), \quad (5)$$

where $F_h = F_s + L_v F_q$.

Note that Eqs. (3)–(5) ignore the horizontal convergence of eddy fluxes of heat and moisture and assume that Reynolds averaging is valid for meso-α heat and moisture budgets. The validity of these approximations deteriorates as the resolution of the analyzed fields increases. However, the horizontal flux convergence due to eddies can be neglected when the eddy statistics are approximately homogeneous over the spatial scale of interest. This appears to be a reasonable first approximation since the mesoscale convective bands in GATE nonsquall cloud clusters vary significantly in their orientation and position with respect to the widespread upper-level anvil clouds (e.g., Leary and Houze, 1979).

We define a virtual flux F_h^* by vertically integrating Eq. (5) to obtain

$$F_h^*(p) = \overline{(Q_1 - Q_2 - Q_R)}. \quad (6)$$

where the overbar refers to the vertical integral

$$\overline{(\ )} \equiv \int_{70}^{p} (\ ) \frac{dp}{g}.$$

The $F_h^*(p)$ will differ from $F_h(p)$ during periods when the vertically integrated cloud-ice content above p is changing. However, since the effect of ice storage will be on the order of Q_2/L_v, and since $L_f \ll L_v$, we expect that $F_h^*(p) \approx F_h(p)$.

When Eqs. (3) and (4) are vertically integrated we obtain

$$\overline{Q_1} = \overline{Q_R} + S_0 + L_v(\overline{C_a + S_c}) + L_f(\overline{d - s + f - m}) \quad (7)$$

$$\overline{Q_2} = -L_v E_0 + L_v(\overline{C_a + S_c}) \quad (8)$$

where C_a is the conversion of airborne water (including water vapor, cloud liquid water and cloud ice) to precipitation and S_c is the apparent large-scale source of cloud water and cloud ice. The S_0 and E_0 are surface fluxes of sensible heat and water vapor, respectively. As noted above, we expect the last term on the right-hand side of Eq. (7) to be negligible in comparison with the other terms.

Surface values of the sensible heat flux and evaporation were also determined independently from the hourly WMO surface data by means of the bulk aerodynamic formulas

$$S_0 = \rho c_p C_T V_a(\theta_0 - \theta_a)$$

$$LE_0 = \rho C_q V_a(q_0 - q_a),$$

where V and θ are the wind speed and potential temperature and the subscripts "0" and "a" refer to values evaluated at the sea surface and 10 m above the surface, respectively. The 10 m values of the transfer coefficients C_T and C_q were computed by the method of Liu et al. (1979).

4. Composite heat and moisture budgets

a. Q_1 and Q_2

Figures 1 and 2 present fields of the large-scale heat source and moisture sink along north–south cross sections through the center of the composite nonsquall system during its growing, mature and dissipating stages. In the growing stage, Q_1 increases rapidly with height below 850 mb and then more slowly to the maximum just above 635 mb. A secondary maximum appears just below 400 mb. Heating in excess of 4°C d^{-1} is confined mainly to the layer below 250 mb. The Q_2 has one large maximum near 890 mb and shows that most of the apparent drying is confined below the 635 mb level in the growing stage.

In the mature stage, the maximum in apparent heating shifts upward by 200 mb to the 430 mb level. The values of the heating are larger than in the growing stage even at the level of the growing-stage heating peak near 635 mb, and the shape of the vertical profile has undergone a very significant change. The lower-tropospheric peak of Q_2 remains about the same magnitude but shifts upward to the 770 mb level. A second drying maximum forms near the 530 mb level in the mature stage to give the Q_2 profile a clear double-peak structure.

In the dissipating stage, the magnitudes of Q_1 and Q_2 decrease dramatically. A heating maximum of about 6°C d^{-1} can be seen near 400 mb. A layer of weak (~3½°C d^{-1}) and relatively uniform heating exists from 600 to 865 mb. Below 865 mb the heating drops to very small positive values. Drying minima now develop at low levels while the drying maximum at upper levels continues to shift upward to near the 430 mb level. A Q_2 minimum with small negative values near the 635 mb level separates the two regions of maximum drying.

The time-dependent behavior of Q_1 in Fig. 1 is consistent with Houze's (1982) discussion of the possible role of the mesoscale anvil clouds in cloud-cluster heat budgets. Houze's model of heating by condensation and radiation within a typical mesoscale updraft and the cooling due to evaporation and melting in the mesoscale downdraft below, gave contributions that were large enough to create a significant upward shift in the location of total heating maximum as the anvil cloud develops. The upward shift of the heating maximum by 200 mb and the 50% increase in magnitude from the growing to the mature stage in Fig. 2 are both in very good qualitative agreement with Houze's estimates. A possible discrepancy is the behavior of the

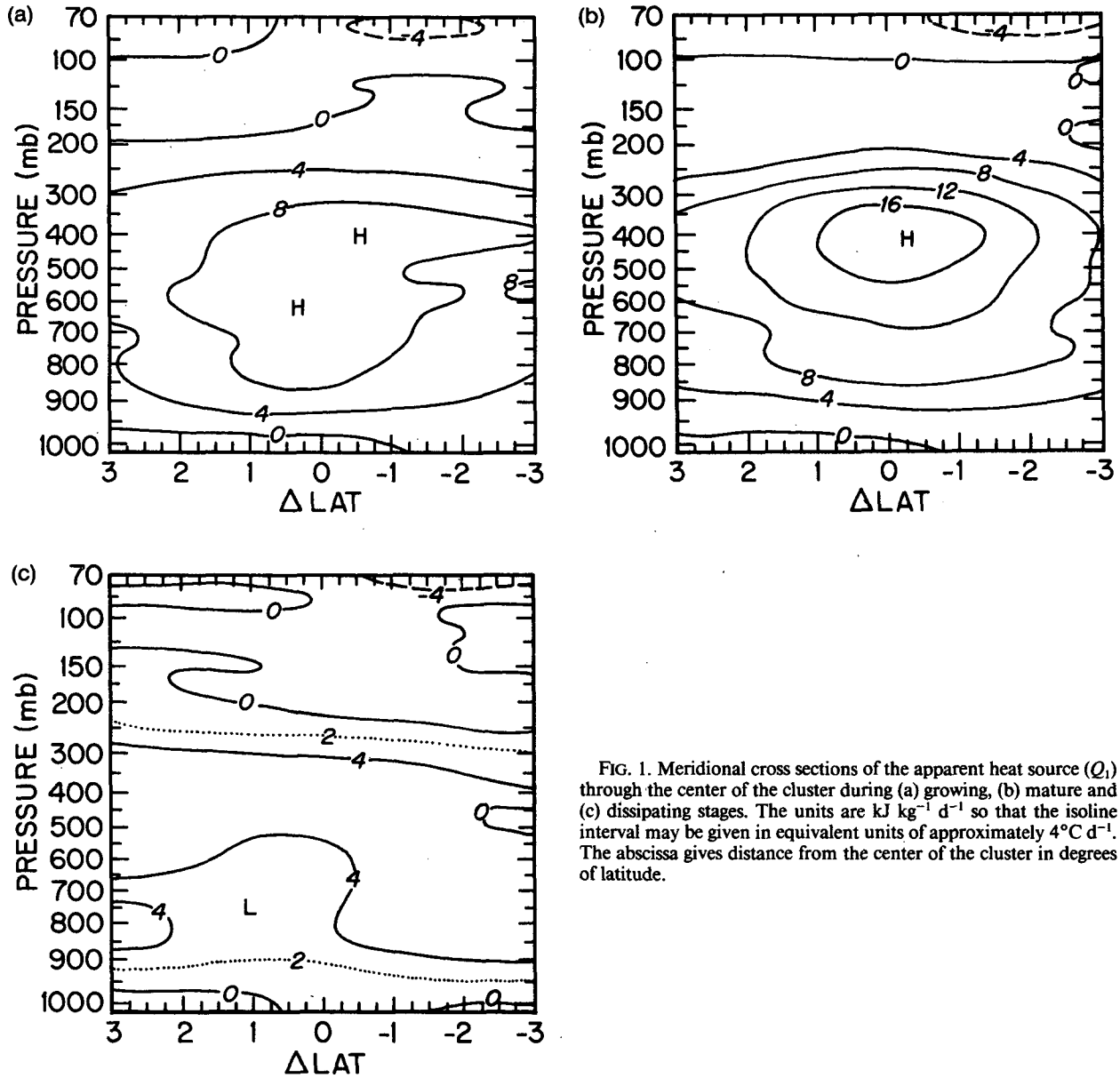

FIG. 1. Meridional cross sections of the apparent heat source (Q_1) through the center of the cluster during (a) growing, (b) mature and (c) dissipating stages. The units are kJ kg^{-1} d^{-1} so that the isoline interval may be given in equivalent units of approximately 4°C d^{-1}. The abscissa gives distance from the center of the cluster in degrees of latitude.

heating profile at lower levels; our budget results indicate that there is no significant decrease in the heating rates in the lower troposphere from the growing to the mature stage. It is possible that the apparent large-scale heating by convective-scale features is overcompensating the cooling due to the mesoscale downdrafts at lower levels as the system matures. The verification of this hypothesis, however, requires a combination of diagnostic analyses and dynamical modeling that are beyond the scope of this investigation.

The double-peak structure of the Q_2 profile in the mature stage is a common feature of large-scale moisture budgets that are averaged over time periods much longer than the lifetimes of individual cloud clusters (e.g., Yanai et al., 1973). Early diagnostic models of cumulus convection give the double-peak structure as a subtle balance between the effects of deep and shallow clouds. No single physical mechanism was found to explain either of the two maxima or the minimum in Q_2, although Chen (1985) gives some evidence for a midtropospheric maximum of detrainment in the GATE area. Recently, however, Johnson (1984) has proposed that the double-peak structure can be explained as the consequence of the distinct and vertically separated drying effects of mesoscale anvils and deep convective cells.

Our results support Johnson's (1984) hypothesis in two ways. First, the upper drying maximum develops

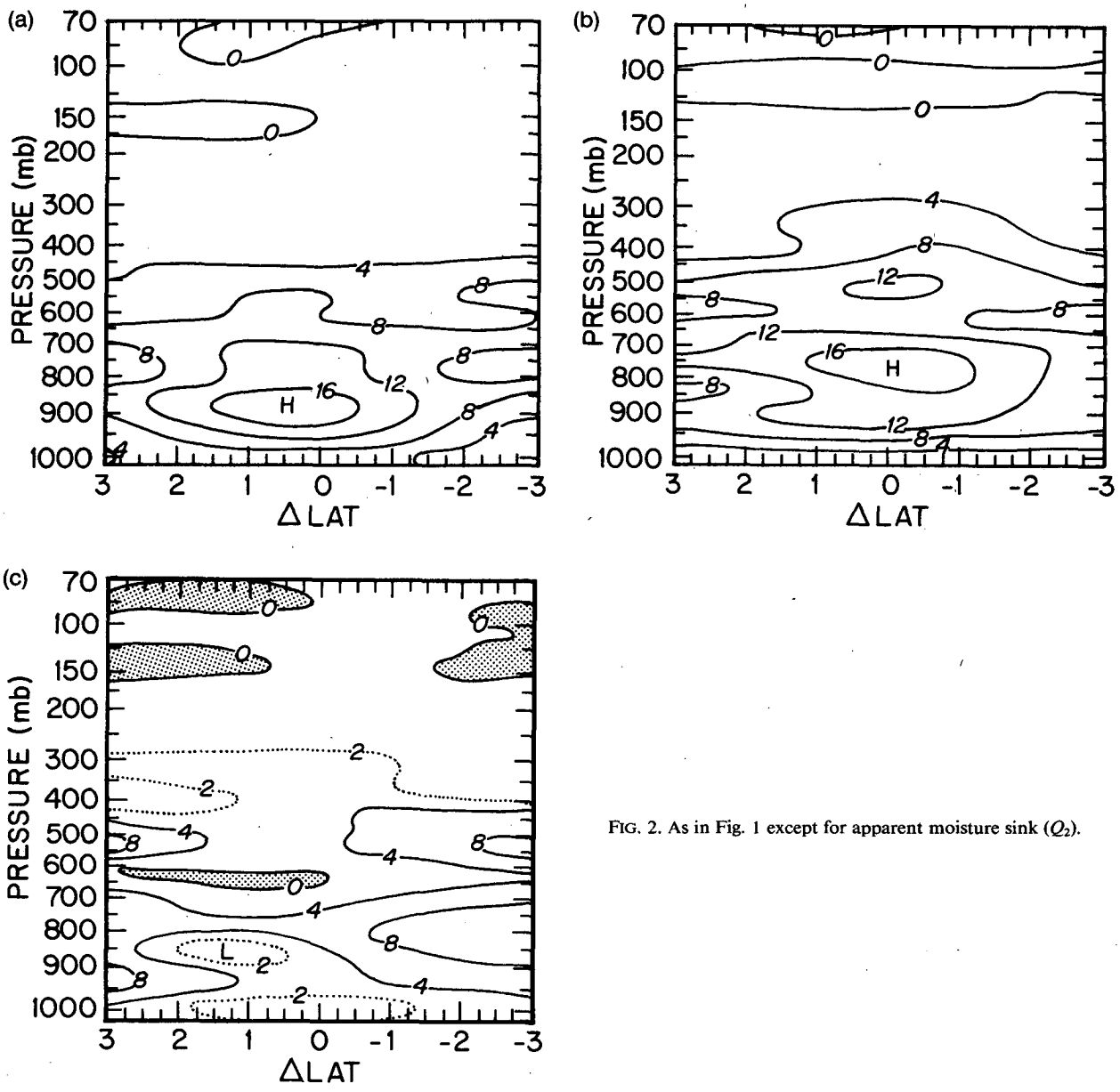

FIG. 2. As in Fig. 1 except for apparent moisture sink (Q_2).

between the growing and the mature stage when strong upward motion and the anvil clouds are developing in the upper troposphere (see Part I). Second, the upward shift in the lower-tropospheric drying maximum between the growing and the mature stage may reflect an increase in the amount of evaporation at low levels beneath the mesoscale anvils.

It is interesting to compare the present results with other time-dependent large-scale heat and moisture budget computations for GATE. We have seen in Part I that all of the convective systems which we have included in our composite occurred at or near the time of easterly wave trough passages. As expected, the heat and moisture budgets of the composite easterly wave in the vicinity of the GATE ship arrays by Thompson et al. (1979) have a number of features in common with the present results. However, the development of a strong upper-tropospheric heat source and a double-peak structure in the large-scale drying is not as pronounced as the trough approaches. Also, the collapse of the drying at lower levels is less dramatic in the case of the composite wave.

The large nonsquall systems included in our composite appear to be strongly influenced by the diurnal cycle. Growing stages tend to occur in the late night and early morning hours, mature stages occur in the middle of the day and dissipating stages tend to occur in the afternoon and evening. This behavior of deep

convection in GATE has been noted by many authors, including Albright et al. (1981), who computed Q_1 and Q_2 as a function of time of day for all three phases of GATE. The Q_1 values in the growing and mature stages of our composite cluster resemble the midday heating profiles of Albright et al. (1981) more strongly than they resemble the easterly wave trough profiles of Thompson et al. (1979); the heating is deeper for our budgets centered on the cloud cluster, with a local maximum appearing in the 500–600 mb layer. Also, the moisture sink at midday more closely resembles the mature stage composite than it does the wave-trough composite.

b. Q_R

Figure 3 shows the Q_R field along a north–south cross section through the center of the composite nonsquall system during its life cycle. In general, the center of the cluster is a region of relatively weak values of the radiative cooling superimposed on a background cooling of -1 to -2°C d^{-1}. In agreement with Byrd and Cox (1984), largest horizontal gradients of radiative cooling are consistently found in the 400–700 mb layer.

Our results show that the largest radiative effects are found in the mature stage of the cloud clusters. Over the center of the array, the magnitude of the radiative

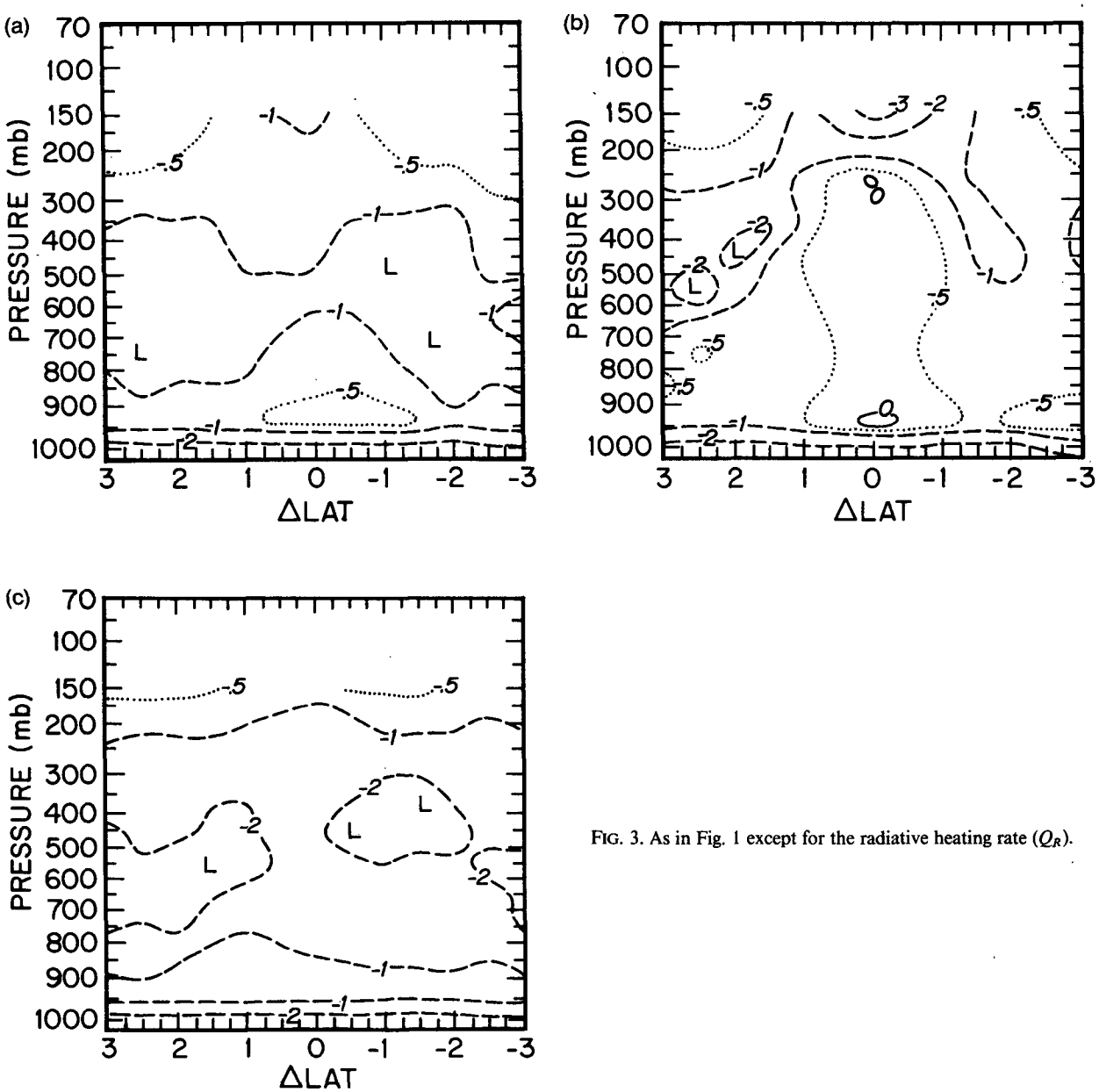

FIG. 3. As in Fig. 1 except for the radiative heating rate (Q_R).

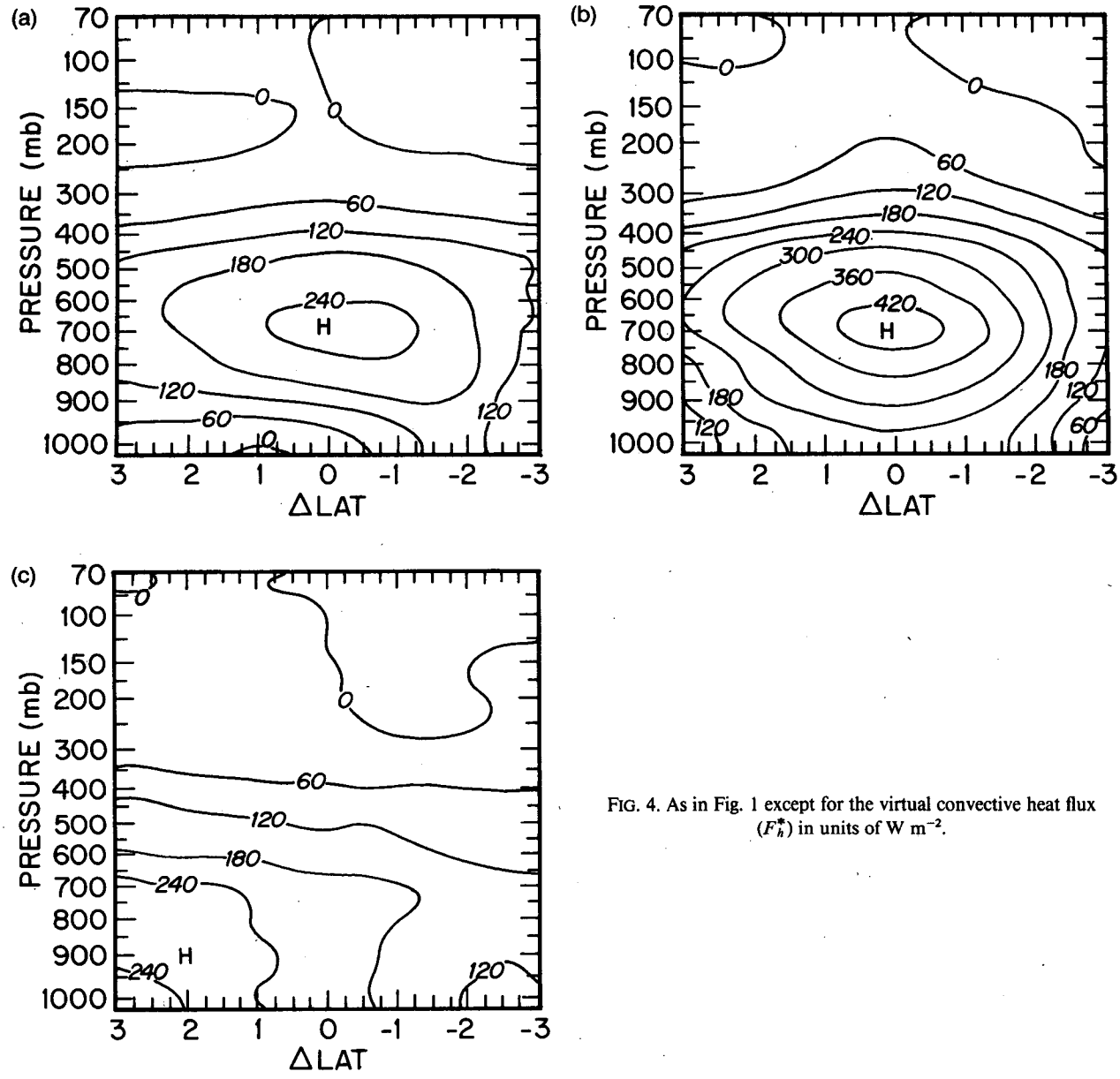

FIG. 4. As in Fig. 1 except for the virtual convective heat flux (F_h^*) in units of W m^{-2}.

cooling is near -0.5°C d^{-1}, and Q_R even becomes positive near 950 and 250 mb. Above 200 mb, the cooling exceeds -3°C d^{-1}, due to enhanced longwave radiative cooling near the top of the upper-level cloud shield.

In their case study of GATE cloud clusters during the 4–6 September 1974 period, Byrd and Cox (1984) reached the conclusion that radiative forcing was strongest during the developing stages of the cluster activity on 5 September, rather than the period of maximum convective activity. The apparent disagreement with our composite result, however, comes from a difference in perspective. Byrd and Cox treated the nighttime convective activity associated with the decaying squall line on 4 September (see Houze, 1977) as part of the formative stage of the 5 September double cluster. Since the horizontal radiative heating gradients due to clouds are largest at night, this gives the impression that radiative forcing is greatest during the development of the 5 September clusters.

In contrast, this study defines cloud clusters by focusing on the evolution of a single, continuous upper-level cloud shield formed by one or more mesoscale precipitation features. With this definition, it is natural that radiative heating gradients will tend to be largest when the anvil cloud is most fully developed, i.e., during the mature stage. While radiation may have played an important role in the evolution of the double cluster on 5 September, our results do not support the con-

tention that this effect is more pronounced in the developing stage of the clusters.

c. F_h^*

Figure 4 presents north–south cross sections of the virtual convective fluxes over the life cycle of the composited nonsquall cloud clusters. The values of F_h^* have been computed using Eq. (6).

In the growing stage, the pattern is dominated by a single flux maximum of 265 W m^{-2} near the 700 mb level at the center of the convective system. This maximum remains at the same location but nearly doubles in magnitude to 451 W m^{-2} in the mature stage. In the dissipating stage, the large maximum disappears completely and is replaced by a constant flux layer extending from the surface to 725 mb.

At upper levels, virtual fluxes in excess of 100 W m^{-2} are generally confined below the 400 mb level. However, in the mature stage, 100 W m^{-2} fluxes can be found above the 300 mb level at the center of the system. The slight bulge in the mature-stage pattern over the center of the array in the 100–300 mb layer is due to the strong radiative cooling near the top of the upper-layer cloud shield.

Near the surface, the virtual fluxes are found to be much larger ($\sim$200 W m^{-2}) in the mature stage and dissipating stage than they are in the growing stage ($\sim$100 W m^{-2}). There is also an apparent shift in the zone of maximum virtual flux to the north as time progresses.

d. *Vertically integrated budgets*

Important information on the general reliability of our budget computations can be obtained from bulk aerodynamic estimates of surface sensible and latent heat fluxes from marine meteorological observations taken aboard the A/B and B array ships. The bulk aerodynamic estimates of S_0 and E_0 at each ship were accumulated on the composite grids and then arithmetically averaged to obtain the mean values shown in Tables 2 and 3. Comparison of $F_h^*(p_s)[\approx F_h(p_s)]$ with $S_0 + L_vE_0$ provides a particularly stringent test since a systematic error of only $c_p \times 1°\text{C d}^{-1}$ in Q_1, Q_2 or Q_R will result in a vertically integrated error on the order of 100 W m^{-2} in the value of $F_h^*(p_s)$.

The budget results and the surface observations summarized in Table 2 show that the surface fluxes of sensible and latent heat reach a maximum in the mature stage. The changes in $S_0 + L_vE_0$ from the growing to the mature stage are much smaller than the difference between the wake of a GATE squall line and its surroundings as computed by Johnson and Nicholls (1983). This is probably due to coarser resolution of the composite grid in this study which averages conditions over a much larger area than the wake of a single mesoscale precipitation feature. Johnson and Nicholls' results show total fluxes in the wake environment of around 50–150 W m^{-2}, with extreme values of 300–500 W m^{-2} just behind the convective line. The bulk aerodynamic estimates in this study are also 50–150 W m^{-2} over most of the composite grid, with extreme values up to 230 W m^{-2}. The small size of the changes with time in the composited $S_0 + L_vE_0$ values are therefore reasonable.

There are, however, considerable quantitative discrepancies between the vertically integrated budget results and the bulk aerodynamic estimates. The budget results underestimate the surface observations by $\sim$20% in the mature and dissipating stages and by $\sim$75% in the growing stage. An underestimate of 20% is probably within the reliability of the bulk aerodynamic formulas and the sampling errors involved in averaging the point measurements of the fluxes on the composite grid; a 75% underestimate indicates a small but systematic error in the total heat budget of the growing stage.

For completeness, Table 3 shows the vertically integrated heat and moisture budgets for the growing, mature and dissipating stages of the composite cluster averaged over the composite grid. As found by Frank (1978) from time series of A/B array budgets, the estimates of the net condensation by the moisture budget exceed those by the heat budget. Unfortunately, the area covered by precipitation estimates from meteorological radar (Hudlow and Patterson, 1979) did not extend over a large enough portion of our composite grid to obtain a reliable composite precipitation field for comparison with the budget quantities in Table 3.

e. *Temperature and moisture structure*

Although the nonsquall cloud clusters have dramatic effects on the meso-α scale mass, heat and moisture budgets, the temporal changes of the temperature and moisture fields over the lifetime of the clusters are dominated by the passage of easterly waves through the GATE ship array. Figure 5 shows the differences of temperature and specific humidity between the growing and dissipating stages of the cloud clusters. Except for a slight decrease of water vapor in the lower troposphere and a weak local maximum of temperature in the 300–400 mb layer, the patterns are large in scale and not centered on the convection. The dominant feature is the increase in water vapor near 600 mb that

TABLE 2. Mean surface flux of F_h^* over the composite grid determined independently from the upper-air heat and moisture budget results and the surface marine meteorological observations.

Stage	Budget results (W m^{-2})	Surface observations (W m^{-2})
Growing	35	150
Mature	131	161
Dissipating	115	145

TABLE 3. Vertically integrated and areally averaged heat and moisture budget components over the composite grid, given in equivalent units of mm d^{-1} and sensible and latent heat flux estimates from surface marine meteorological observations. Note that 1 mm d^{-1} of surface evaporation is approximately equivalent to a latent heat flux of 28.7 W m^{-2}.

Stage	$\overline{(Q_1 - Q_R)}$	$\overline{Q_2}$	S_0	L_vE_0	$\overline{(Q_1 - Q_R)} - S_0$	$\overline{Q_2} + L_vE_0$
Growing	22:2	21.0	0.6	4.6	21.6	25.6
Mature	26.3	21.8	0.7	4.9	25.6	26.7
Dissipating	18.6	14.6	0.6	4.5	18.0	19.1

is a well-known feature of the easterly waves passing through the GATE ship arrays (Thompson et al., 1979), with maximum amplitudes in the northern part of the array.

5. Conclusions and discussion

In this study we have examined the heat and moisture budgets on the meso-α scale during the life cycles

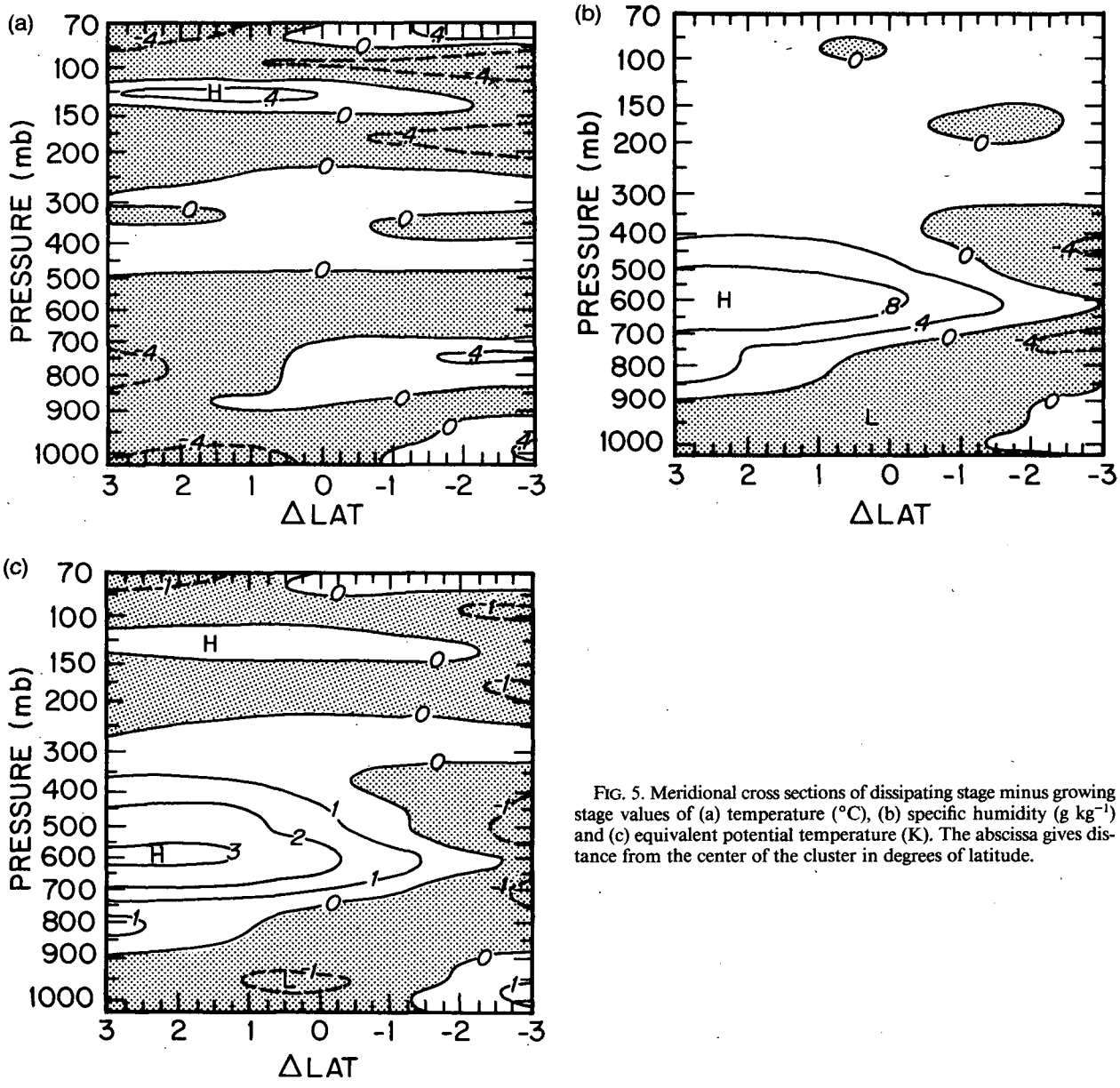

FIG. 5. Meridional cross sections of dissipating stage minus growing stage values of (a) temperature (°C), (b) specific humidity (g kg^{-1}) and (c) equivalent potential temperature (K). The abscissa gives distance from the center of the cluster in degrees of latitude.

of five large nonsquall cloud clusters that formed over the dense ship array during Phase 3 of GATE. The time-dependent behavior of the budgets give support to the hypothesis of Leary and Houze (1979) that the widespread upper-level cloud decks associated with cloud clusters play an active and important role in determining the large-scale heat and moisture budgets.

We find evidence in the growing stage for strong convective activity, with a very large low-level, large-scale moisture sink separated in height from the regions where the large-scale heating is realized. In the mature stage, the upward shift and the strong development of the apparent heating in the 500 to 600 mb layer, as well as the corresponding development of a secondary maximum of apparent drying, is consistent with the existence of a dynamically active anvil cloud. Our composite of radiative heating estimates by Cox and Griffith (1979) also shows that horizontal radiative heating gradients reach their maximum strength in the mature stage. In the dissipating stage, the results show that the large-scale apparent heat source is approximately balanced by the apparent moisture sink above the freezing level, suggesting the existence of large-scale condensation in the anvil.

The vertical flux of sensible and latent heat below the scale of our analysis has a large maximum near 700 mb in the center of the convective system in the growing and mature stages of the cluster. This is the total heat transport that connects the lower-tropospheric region where the large-scale flow appears to lose heat with the upper-tropospheric region where heat is gained. This flux nearly doubles in the mature stage. The flux in the dissipating stage, however, appears to be confined to the layer below the freezing level, as would be expected during the boundary layer recovery.

One of the most interesting remaining problems is explaining the mechanism and the timing of the clear diurnal signal in the mass, heat and moisture budgets during GATE. The life cycle of the nonsquall clusters in this study are clearly related to the diurnal variations in the large-scale heat and moisture budgets computed by Albright et al. (1981).

The synoptic environment of the clusters certainly must play a role in the diurnal variation of the convective activity, even if the role is indirect. For example, the nonsquall systems during Phase 3 of GATE existed in a synoptic environment having very little vertical wind shear in the lower troposphere. Without wind shear the MPFs were apparently unable to propagate rapidly enough to obtain a continuous supply of energy-rich boundary layer air. Thus, even without a diurnal cycle, the convection associated with large anvil clouds would have had a lifetime on the order of the boundary-layer recovery period (Ooyama, 1982). But the imbalance between the synoptic-scale supply of moisture on the one hand and the mesoscale and convective-scale consumption of moisture on the other is inadequate to explain the clear diurnal timing of the cloud systems.

It also seems obvious that the interaction of radiation with the clouds must be important in determining the diurnal statistics of deep convective systems. Gray and Jacobson (1977) have proposed that the vertical convergence profile observed in tropical weather systems is maintained and diurnally modified by differences between the radiation–condensation heating profiles in a region covered by a thick upper-level cloud shield and the surrounding clear areas.

Byrd and Cox (1984) show that the horizontal radiative heating gradients associated with the GATE cloud clusters on 4–6 September were greatest at night. But the large spatial variations in the intensity and timing of deep convection with respect to the solar cycle documented by McBride and Gray (1980) and McGarry and Reed (1978) indicate that the full quantitative explanation of the timing may be quite complex. Fortunately, the strength of the signal found over the GATE ship arrays is quite strong. Combined observational and theoretical studies on this subject may therefore be feasible and quite enlightening.

Acknowledgments. The authors would like to thank K. V. Ooyama for his support and perseverance in the analysis of the GATE surface and upper-air datasets. We are also grateful to S. K. Cox for providing the radiation data.

The staff of the Department of Atmospheric Sciences and the Climatic Research Institute provided us with excellent support. W. McKie and R. Mobley acted as computing consultants and M. Burrier typed the manuscript. K. Torvik drafted the figures.

This material is based upon work supported by the National Science Foundation under Grants ATM-8213130 and ATM-8414820.

REFERENCES

Albright, M. D., D. R. Mock, E. E. Recker and R. J. Reed, 1981: A diagnostic study of the diurnal rainfall variation in the GATE B-scale area. *J. Atmos. Sci.*, **38,** 1429–1445.

Byrd, G. P., and S. K. Cox, 1984: A case study of radiative forcing upon a tropical cloud cluster system. *Mon. Wea. Rev.*, **112,** 173–187.

Chen, Y.-L., 1985: Diagnosis of the net cloud mass flux in GATE. *J. Atmos. Sci.*, **42,** 1757–1769.

Cox, S. K., and K. T. Griffith, 1979: Estimates of radiative divergence during Phase III of the GARP Atlantic Tropical Experiment: Parts I and II. *J. Atmos. Sci.*, **36,** 576–601.

Frank, W. M., 1978: The life cycles of GATE convective systems. *J. Atmos. Sci.*, **35,** 1256–1264.

——, 1979: Individual time period analyses over the GATE ship array. *Mon. Wea. Rev.*, **107,** 1600–1616.

Gray, W. M., and R. W. Jacobson, Jr., 1977: Diurnal variation of deep cumulus convection. *Mon. Wea. Rev.*, **105,** 1171–1188.

Houze, R. A., Jr., 1977: Structure and dynamics of a tropical squall-line system observed during GATE. *Mon. Wea. Rev.*, **105,** 1540–1567.

——, 1982: Cloud clusters and large-scale vertical motions in the tropics. *J. Meteor. Soc. Japan,* **60,** 396–410.

Hudlow, M. D., and V. L. Patterson, 1979: GATE Radar Rainfall Atlas. NOAA Spec. Rep., Center for Environmental Assessment Services, NOAA, 155 pp. [Govt. Printing Office Stock No. 003-019-00046-2].

Johnson, R. H., 1984: Partitioning tropical heat and moisture budgets into cumulus and mesoscale components: Implications for cumulus parameterization. *Mon. Wea. Rev.*, **112,** 1590–1601.

——, and M. E. Nicholls, 1983: A composite analysis of the boundary layer accompanying a tropical squall line. *Mon. Wea. Rev.*, **111,** 308–319.

——, and G. S. Young, 1983: Heat and moisture budgets of tropical mesoscale anvil clouds. *J. Atmos. Sci.*, **40,** 2138–2147.

Leary, C. A., and R. A. Houze, Jr., 1979: The structure and evolution of convection in a tropical cloud cluster. *J. Atmos. Sci.*, **36,** 437–457.

Liu, W. T., K. B. Katsaros and J. A. Businger, 1979: Bulk parameterization of air-sea exchanges of heat and water vapor including the molecular constraints at the interface. *J. Atmos. Sci.*, **36,** 1722–1735.

McBride, J. L., and W. M. Gray, 1980: Mass divergence in tropical weather systems. Paper I: Diurnal variation. *Quart. J. Roy. Meteor. Soc.*, **106,** 501–516.

McGarry, M. M., and R. J. Reed, 1978: Diurnal variations in convective activity and precipitation during Phases II and III of GATE. *Mon. Wea. Rev.*, **106,** 101–113.

Ooyama, K., 1982: Conceptual evolution of the theory and modeling of the tropical cyclones. *J. Meteor. Soc. Japan,* **60,** 369–379.

——, 1987: Scale-controlled objective analysis. *Mon. Wea. Rev.*, **115** 2479–2506.

Reeves, R. W., and S. K. Esbensen, 1977: GATE workshop recommendations for integrating U.S.S.R. RKZ and U.S. VIZ rawinsonde thermodynamic observations. Report of the U.S.A. Workshop on the GATE Central Program, 25 July–12 August 1977, NCAR, Boulder, CO, pp. 165–168.

Riehl, H., and J. S. Malkus, 1958: On the heat balance in the equatorial trough zone. *Geophysica,* **6,** 503–538.

Thompson, R. M., Jr., S. W. Payne, E. E. Recker and R. J. Reed, 1979: Structure and properties of synoptic-scale wave disturbances in the intertropical convergence zone of the eastern Atlantic. *J. Atmos. Sci.*, **26,** 53–72.

Tollerud, E. I., and S. K. Esbensen, 1983: An observational study of the upper-tropospheric vorticity fields in GATE cloud clusters. *Mon. Wea. Rev.*, **111,** 2161–2175.

——, and ——, 1985: A composite life cycle of nonsquall mesoscale convective systems over the tropical ocean. Part I: Kinematic fields. *J. Atmos. Sci.*, **42,** 823–837.

Yanai, M., S. K. Esbensen and J.-H. Chu, 1973: Determination of bulk properties of tropical cloud clusters from large-scale heat and moisture budgets. *J. Atmos. Sci.*, **30,** 611–627.